J|A|C|S
ARTICLES
Published on Web 09/02/2005

# Pd-Mediated Activation of Molecular Oxygen in a Nonpolar Medium

Jason M. Keith, Robert J. Nielsen, Jonas Oxgaard, and William A. Goddard III*

*Contribution from the Materials Process and Simulation Center, Beckman Institute (139-74), California Institute of Technology, Pasadena, California 91125*

Received November 16, 2004; E-mail: wag@wag.caltech.edu

***Abstract:*** The mechanism for direct insertion of $O_2$ in a toluene-solvated palladium−hydride bond (avoiding palladium zero) has been elucidated using quantum mechanics (B3LYP/LACVP** with the PBF polarizable continuum solvent model) for $Pd^{II}$((−)-sparteine)(Cl)(H) and the model compound $Pd^{II}$(bipyridine)(Cl)(H). We find that the process involves (1) the abstraction of the hydrogen atom by triplet oxygen, (2) the formation of a stable $L_2XPd^{I}OOH$ triplet species, (3) a spin transition resulting in a stable $L_2XPd^{II}OOH$ singlet species, and (4) the loss of $H_2O_2$ and completion of the catalytic cycle upon the addition of HX. The limitations involved in the spin transition, the formation of the triplet $Pd^{I}$−OOH species and the stability of that triplet species are all dependent on the presence of an H-bond acceptor cis to the hydride and the electronic characteristics of the other ligands which may or may not stabilize the $Pd^{I}$ species. Without this cis H-bond acceptor and/or electron-withdrawing ligands that can stabilize $Pd^{I}$, the reaction will not proceed via the palladium hydride insertion mechanism in a nonpolar environment.

## 1. Introduction

Homogeneous catalytic systems involving $Pd^{II}$ complexes have been used as efficient oxidization catalysts with the use of molecular oxygen as a terminal oxidant.[1−4] Molecular oxygen is an ideal oxidant due to its availability, its solubility in common solvents, and its production of environmentally safe byproducts such as water and hydrogen peroxide, itself a commercially important chemical. Despite its importance, the mechanistic details of the involvement of $O_2$ in these processes are largely unknown.

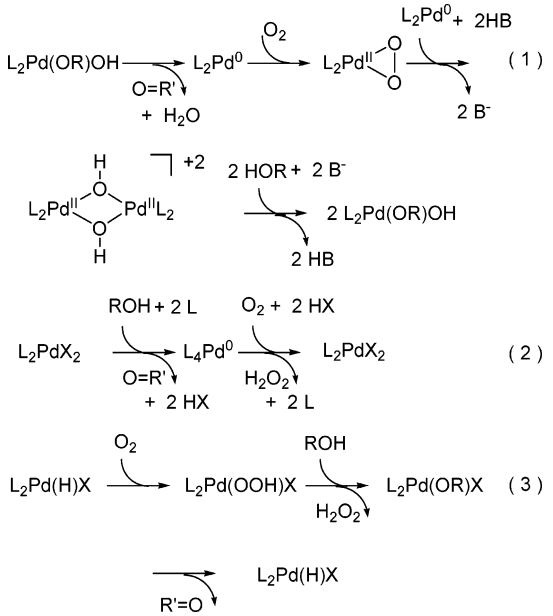


There are currently three major mechanistic proposals to explain the role of dioxygen in these processes. The first two mechanisms, as proposed by Sheldon[2] (eq 1) and Bianchi[3] (eq 2), proceed via a $Pd^0$ intermediate, which subsequently reacts with the dioxygen. The third mechanism, as proposed by Hosokawa and Murahashi (eq 3), postulates the direct insertion of $O_2$ in a Pd−H bond, thus avoiding $Pd^0$ altogether.[4] Later experimental work by Stahl suggested a variant of eq 1 where the $L_2PdO_2$ species is protonated directly, thus avoiding dimerization.[5]

As part of our work on Pd-catalyzed oxidation of alcohols in nonpolar media,[6] we investigated the interaction of $O_2$ with $Pd^{II}$ hydride in a direct insertion mechanism. While alternative $Pd^0$ mechanisms are currently under investigation, we have found that the direct insertion is indeed plausible, but only for a select subset of Pd complexes. In this report we will demonstrate a detailed mechanistic picture and discuss the

(1) (a) Peterson, K. P.; Larock, R. C. *J. Org. Chem.* **1998**, *63*, 3185. (b) Ferreira, E. M.; Stoltz, B. M. *J. Am. Chem. Soc.* **2001**, *123*, 7725. (c) Jensen, D. R.; Pugsley, J. S.; Sigman, M. S. *J. Am. Chem. Soc.* **2001**, *123*, 7475. (d) Steinhoff, B. A.; Fix, S. R.; Stahl, S. S. *J. Am. Chem. Soc.* **2002**, *124*, 766. (e) Steinhoff, B. A.; Stahl, S. S. *Org. Lett.* **2002**, *4*, 4179.
(2) ten Brink, G.-J.; Arends, I. W. C. E.; Sheldon, R. A. *Science* **2000**, *287*, 1636.
(3) Bortolo, R.; Bianchi, D.; D'Aloisio R.; Querci, C.; Ricci, M. *J. Mol. Catal. A* **2000**, *153*, 25.
(4) (a) Nishimura, T.; Uemura, S. *Synlett* **2004**, *2*, 201. (b) Nishimura, T.; Onoue, T.; Ohe, K.; Uemura, S. *J. Org. Chem.* **1999**, *64*, 6750. (c) Nishimura, T.; Onoue, T.; Ohe, K.; Uemura, S. *Tetrahedron Lett.* **1998**, *39*, 6011. (d) Hosokawa, T.; Murahashi, S.-I. *Acc. Chem. Res.* **1990**, *23*, 49.
(5) (a) Steinhoff, B. A.; Guzei, I. A.; Stahl, S. S. *J. Am. Chem. Soc.* **2004**, *126*, 11268. (b) Konnick, M. M.; Guzei, I. A.; Stahl, S. S. *J. Am. Chem. Soc.* **2004**, *126*, 10212. (c) Stahl, S. S.; Thorman, J. L.; Nelson, R. C.; Kozee, M. A. *J. Am. Chem. Soc.* **2001**, *123*, 7188.
(6) Nielsen, R. J.; Keith, J. M.; Stoltz, B. M.; Goddard, W. A., III. *J. Am. Chem. Soc.* **2004**, *126*, 7967.


**10.1021/ja043094b CCC: $30.25** 

structural requirements of this process, as well as introduce some new aspects of the triplet−singlet crossover involved.

## 2. Computational Methodology

All calculations were performed using the hybrid DFT functional B3LYP as implemented by the Jaguar 5.5 program package.[7] This DFT functional utilizes the Becke three-parameter functional[8] (B3) combined with the correlation functional of Lee, Yang, and Parr[9] (LYP), and is known to produce good descriptions of reaction profiles for transition-metal-containing compounds.[10,11] Pd was described with the LACVP** effective core potential and basis set (18 explicit electrons).[12] All other elements were described including the core electrons, using the Pople 6-31G** basis set,[13] but with 3s combination of the six d-like functions reduced to five. Diffuse functions were also added to Cl. The resulting basis set is denoted LACVP**(a).

All geometries were optimized and evaluated for the correct number of imaginary frequencies through vibrational frequency calculations using the analytic Hessian. Zero imaginary frequencies correspond to a local minimum, while one imaginary frequency corresponds to a transition structure.

Implicit solvent effects were calculated with the Poisson−Boltzmann (PBF) continuum approximation,[14] using the parameters $\epsilon = 2.379$ and solvent radius = 2.762 Å. Here we use the solvent-accessible surface of the molecular complex built using standard van der Waals radii. The solvation effects were calculated at geometries optimized for the gas phase.

Using the analytic Hessian, we calculated the zero-point energy corrections at 0 K and added this to the solvation correction and the QM energy [$\Delta(E)$]) to obtain the enthalpy at 0 K [$\Delta H(0\text{ K})$]. Similarly, the vibrational frequencies were used to calculate the entropy and enthalpy corrections to 278.15 K, to obtain $(\Delta H - T\Delta S) = \Delta G(278.15\text{ K})$.

On the basis of previous results, we expect that relative energies on the $\Delta H(0\text{ K})$ surface are accurate to ∼3 kcal/mol for stable intermediates, and to ∼5 kcal/mol for transition structures. Probably the relative energies on the $\Delta G(298\text{ K})$ surface are less accurate, due to the use of the PBF model.[15]

DFT is formulated in terms of Slater determinants built from Kohn−Sham orbitals that are calculated self-consistently. This process is consistent for states that are well described with closed-shell orbitals (up and down spins in the same orbitals), the normal situation for most DFT applications. However, in the studies reported here it was necessary to consider triplet states. With DFT this is done by having two more spin-orbitals with up spin than down spin (unrestricted DFT or UDFT). We refer to this as the triplet state, but it need not be an eigenstate of the spin operator, $\mathbf{S}^2$. Rather it is an eigenfunction of $S_z$, leading to $M_S = 1$. The problem with this formulation occurs when it is necessary to consider transitions between triplet and singlet states, the topic of this paper. Thus, starting with the true triplet orbitals of $O_2$ and calculating the energy of the singlet state should lead to a component of $^1\Delta_g$, with an excitation energy of 22.5 kcal/mol. In fact, UDFT gives an excitation energy of 10.5 kcal/mol. The reason is that the $M_S = 0$ wave function we consider to describe the singlet state also has a component of triplet character. This can be treated by applying the spin projection operator, which leads to true singlet excited state and singlet−triplet splitting of 20.5 kcal/mol,[16a] nearly twice the value from UDFT.[16b] In this paper all results are UDFT, and hence for triplet ground states the excitation energies to the excited singlet state is expected to be about half the rigorous value.[16b]

## 3. Results and Discussion

**3.1. Pd(sparteine) Mechanism. 3.1.1. Triplet H Abstraction−Dioxygen Rotation Mechanism for Dioxygen Insertion.** As the starting point for this study we chose (−)-sparteine−$Pd^{II}(H)(Cl)$ (**1**, Figure 1). Introducing (triplet) molecular oxygen to **1** leads immediately to the formation of a weakly bound van der Waals complex [(spar)$Pd^{II}(H)(Cl)$]·$O_2$ (**2**), with $\Delta H = -0.8$ kcal/mol. There is negligible electron transfer between the $O_2$ and the Pd complex (the Mulliken charges on the two oxygens change from 0 and 0 to 0.06 and −0.02 electron, with the positive charge oxygen closest to the hydride, while the Pd gains 0.04 electron). Spin analysis shows that all unpaired spins in **2** are on the $O_2$ fragment (one $\pi^*$ orbital in the plane, hereafter the $\sigma$ electron, and the other $\pi^*$ orbital perpendicular to the plane, hereafter the $\pi$ electron).

The corresponding fully optimized singlet species is significantly higher in energy ($\Delta H = 9.5$ kcal/mol), indicating that the spin transition cannot occur at this stage in the reaction mechanism. Similar to $O_2$, discussed above in section 2, the UDFT calculation for the $M_S = 0$ or "singlet" state of **2** is contaminated with a significant amount of triplet character, leading to an energy that is far too low.[16]

From **2** we find an unexpected mechanism for $O_2$ insertion. Here the transition state, **TS1** (Figure 2a), has the triplet O2 positioned to abstract the H from the Pd. Thus from **1** to **TS1** the Pd−H bond length stretches from 1.52 to 1.68 Å, indicating a decrease in bond order from 1 to ∼0.7. At the same time the O−O bond distance increases from 1.21 to 1.26 Å, indicating a decrease in bond order of ∼0.2. On the other hand, the O−H distance of 1.33 Å (compared to 0.96 Å in $HO_2$) indicates the O−H bond has not yet formed. At this point the $\pi$ unpaired spin (perpendicular to the $O_2$−H−Pd plane) remains on the $O_2$, while the $\sigma$ unpaired spin (in the plane) has partly delocalized onto the Pd $d_{x^2-y^2}$ orbital (where Pd−H is the $x$ direction and the plane is the $xy$ plane; this orbital is shown in Figure 3). Spin population (shown in Figure 3) for the $O_2$ moiety is 1.53 (equally distributed across both O's), and that for Pd is 0.38.

From **TS1** the energy falls monotonically by 19.1 kcal/mol while the $HO_2$ rotates in the plane to form **3A** (further discussed in section 3.1.3), in which the H is now bonded to the inner O (H−O = 1.02 Å) while the outer O is now bonded to the Pd (Pd−O = 2.25 Å). Here the two unpaired spin orbitals are

(7) *Jaguar 5.5*; Schrodinger, Inc.: Portland, OR, 2003.
(8) Becke, A. D. *J. Chem. Phys.* **199**3, *98*, 5648.
(9) Lee, C.; Yang, W.; Parr, R. G. *Phys. Rev. B* **1988**, *37*, 785.
(10) Baker, J.; Muir, M.; Andzelm, J.; Scheiner, A. In *Chemical Applications of Density-Functional Theory*; Laird, B. B., Ross, R. B., Ziegler, T., Eds.; ACS Symposium Series 629; American Chemical Society: Washington, DC, 1996.
(11) Niu, S.; Hall, B. M. *Chem. Rev.* **2000**, *100*, 353.
(12) (a) Hay, P. J.; Wadt, W. R. *J. Chem. Phys.* **1985**, *82*, 299. (b) Goddard, W. A., III. *Phys. Rev.* **1968**, *174*, 659. (c) Melius, C. F.; Olafson, B. O.; Goddard, W. A., III. *Chem. Phys. Lett.* **1974**, *28*, 457.
(13) (a) Hariharan, P. C.; Pople, J. A. *Chem. Phys. Lett.* **1972**, *16*, 217. (b) Francl, M. M.; Pietro, W. J.; Hehre, W. J.; Binkley, J. S.; Gordon, M. S.; DeFrees, D. J.; Pople, J. A. *J. Chem. Phys.* **1982**, *77*, 3654.
(14) (a) Tannor, D. J.; Marten, B.; Murphy, R.; Friesner, R. A.; Sitkoff, D.; Nicholls, A.; Ringnalda, M.; Goddard, W. A., III; Honig, B. *J. Am. Chem. Soc.* **1994**, *116*, 11875. (b) Marten, B.; Kim, K.; Cortis, C.; Friesner, R. A.; Murphy, R. B.; Ringnalda, M. N.; Sitkoff, D.; Honig, B. *J. Phys. Chem.* **1996**, *100*, 11775.
(15) (a) Truong, T. N.; Truong, T. T.; Stefanovich, E. V. *J. Chem. Phys*. **1997**, *107*, 1881. (b) Cramer, C. J.; Thrular, D. G. *Chem. Rev*. **1999**, *99*, 2161. (c) Oxgaard, J.; Muller, R. P.; Periana, R. A.; Goddard, W. A. III. *J. Am. Chem. Soc*. **2004**, *126*, 352

(16) Similar to $O_2$, the unrestricted singlet species of **2** and **TS1** have $\mathbf{S}^2$ values of 1.004 and 1.017, demonstrating significant spin contamination, and therefore the energy gaps of 9.5 and 5.2 kcal/mol are both underestimated by ∼10 and ∼5 kcal/mol, respectively, although spin projections were not performed. In the singlet hydroperoxo species, **4**, spin contamination is not present ($\mathbf{S}^2 = 0.000$). For further discussion on spin projections of singlet dioxygen, see: (a) Xu, X.; Goddard W. A. *Proc. Natl. Acad. Sci. U.S.A.* **1996**, *99*, 15308. Wittbrodt, J. M.; Schlegel, H. B. *J. Chem. Phys.* **1996**, *105*, 6574. For methods on correcting spin contamination in DFT, see: (b) Bally, T.; Borden, W. T. *Rev. Comput. Chem.* **1999**, *13*, 1.

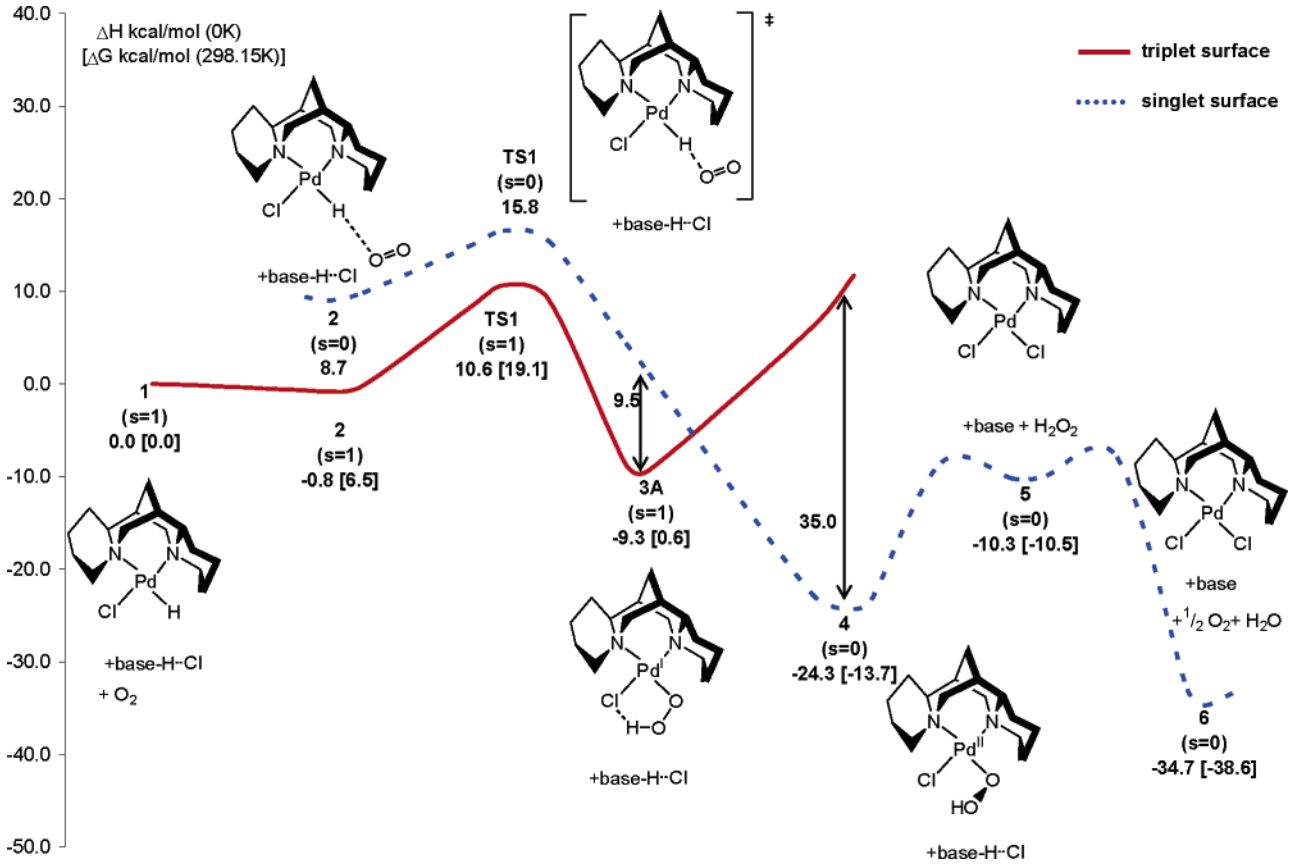


***Figure 1.*** Calculated mechanism for $O_2$ insertion in Pd(spar)(H)(Cl) in toluene (base = spar). Here the triplet surface is shown by the solid (red) line while the singlet surface is shown with the dotted (blue) line. The triplet−singlet crossing between **3A** and **4** is discussed in section 3.3 and shown in Figure 5.

similar to species **TS1**, in which the $\pi$ unpaired spin remains on the $O_2$, while the $\sigma$ unpaired spin (in the plane) has further delocalized onto the Pd $d_{x^2-y^2}$ orbital. The $\Delta H^{\ddagger}$ for **TS1** is 10.6 kcal/mol.

In this **TS1** structure the corresponding UDFT singlet state is higher than the triplet state by 5.2 kcal/mol ($\Delta H$ = 15.8 kcal/mol[16]). This species is contaminated with a significant amount of triplet character, leading to an energy that is far too low,[16] demonstrating that a spin transition need not occur in the $O_2$ insertion step.

**3.1.2. Alternative Mechanisms.** Initially we assumed that the mechanism might proceed through a 2 + 2-like transition state in which the Pd−O and O−H bonds are formed simultaneously with the Pd−H bond being broken. After initial failures to find such a transition state, we carried out geometry searches in which we constrained the Pd−O distance at successively shorter bond lengths from 5.0 to 2.0 Å. However, we found that the energy increased as the distance decreased until the $\Delta H$ was above 18.9 kcal/mol by the point at which Pd−O = 2.0 Å. As an alternative we constrained the Pd−O and Pd−H distances simultaneously (Pd−O from 2.0 to 5.0 Å and Pd−H from 1.5 to 3.5 Å), with similarly negative results.

We also examined the stepwise process in which a five-coordinate Pd species is first formed followed by an insertion. However all attempts to find a stable five-coordinate intermediate were unsuccessful, with the geometries collapsing to Pd(H)(Cl) + $O_2$. These attempts included cases in which the H, Cl, and $O_2$ in turn were each placed in the axial position in a square pyramidal geometry as well as several trigonal bipyramidal geometries.

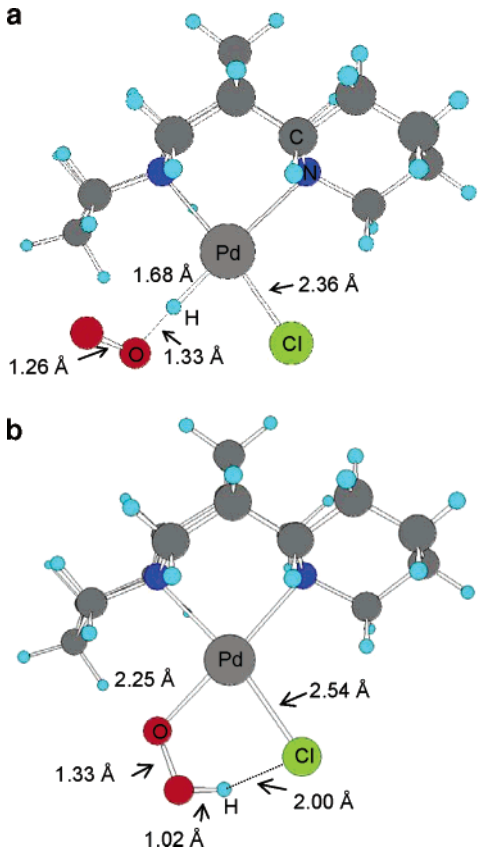


***Figure 2.*** (a) Transition-state structure (**TS1**) for hydrogen abstraction/$O_2$ insertion mechanism. (b) Triplet species **3A**.

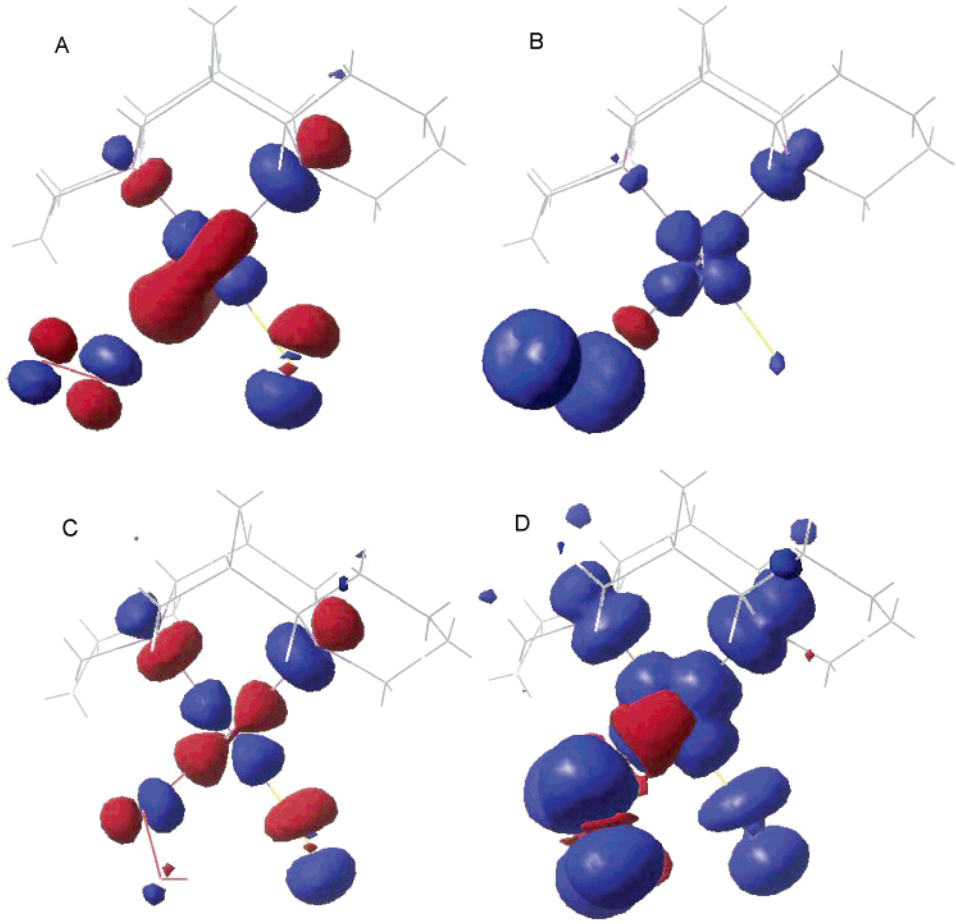


***Figure 3.*** Highest SOMO orbital and spin densities for **TS1** and **3A**, illustrating the contribution from the Pd $d_{x^2-y^2}$. (A) Highest SOMO for **TS1**. (B) Spin distribution of **TS1**. (C) Highest SOMO of **3A**. (D) Spin distribution of **3A**.

Only by allowing the $O_2$ to move away from the metal center and varying the O−H distance with no other constraints were we able to find the mechanism described in section 3.1.1.

**3.1.3. The 3A Intermediate.** The mechanism through **TS1** leads to the planar Pd−OOH species **3A** (Figure 2b), with a $\Delta H$ of −9.3 kcal/mol with respect to **1**. The triplet state in **3A** is best described as a square planar $Pd^{I}$ radical (unpaired spin in the Pd $d_{x^2-y^2}$ orbital; this orbital shown in Figure 3) complexed with the $HO_2^{\bullet}$ peroxyl radial ($\pi$ orbital perpendicular to the plane) acting as a donor ligand. The spin density (shown in Figure 3) for the $O_2$ moiety is 0.98 (0.66 of which resides on the O nearest Pd), and that for Pd is 0.77. Since the unpaired orbitals are orthogonal by symmetry and localized on different centers, they have little interaction and **3A** is a biradical. Indeed, the Pd−O bond distance of 2.25 Å indicates a weak donor−acceptor bond, compared to the significantly shorter value of 2.09 Å expected for a $Pd^{II}$−O single bond.[17] The O−O bond distance of 1.33 Å is typical of a peroxyl radical species (O−O = 1.33 Å in free $HO_2$), halfway between common single and double bond distances of 1.48 and 1.21 Å. The O−H bond distance of 1.02 Å is similar to that of free $HO_2^{\bullet}$ (1.00 Å). Finally, the Pd−Cl bond distance of 2.54 Å and the Pd−N distances of 2.30 (trans to Cl) and 2.35 Å (cis to Cl) are elongated by 0.25, 0.19, and 0.24 Å compared to the bond lengths in other $Pd^{II}$ complexes,[18] as expected for a $Pd^{I}$ center. An interesting feature of **3A** is the H−Cl distance of 2.00 Å between the Cl and the H of the peroxyl radical, which indicates some internal hydrogen bonding. We find that this contributes to the exothermicity of this part of the reaction by significantly stabilizing this intermediate.

In the optimum geometry for the triplet state, the single state for **3A** is 9.5 kcal/mol higher in energy (spin contamination is negligible at this point, with $\mathbf{S}^2 = 0.020$).

**3.1.4. Transition from Triplet to Singlet (3A to 4).** Given the $O_2$ $\pi$ and Pd $d_{x^2-y^2}$ unpaired orbitals of triplet **3A**, we expect the transition to the singlet to occur by merely rotating the $HO_2$ about the O−O axis, where it can overlap the Pd $d_{x^2-y^2}$ unpaired orbital and start bonding to form the final Pd−O bond. This leads to **4**, with $\Delta H = -24.3$ kcal/mol. **4** is clearly a $Pd^{II}$−OOH complex: the Pd−O bond distance of 1.97 Å is consistent with the covalent Pd−O bond in similar species,[17] while the O−O bond distance of 1.43 Å is slightly shorter than a normal single bond distance of 1.48 Å. The O−H bond distance of 0.98 Å is consistent with an O−H bond distance in $H_2O_2$. The Pd−Cl bond distance of 2.42 Å and the Pd−N distances of 2.19 (trans to Cl) and 2.24 Å (cis to Cl) are as expected for $Pd^{II}$.

**3.1.5. Completion of the Catalytic Cycle.** The catalytic cycle is completed with protonation of **4** by an external acid (in this

(17) A bond length of 2.09 Å was observed for $Pd^{II}$−O in (4-vinylpyridine)-[2-[2-acetyl-2-(ethoxycarbonyl)ethyl]-8-quinolinol-*C,N,O*]palladium(II): Kitamura, C.; Inoue, T.; Kawatsuki, N.; Yoneda, A. *Anal. Sci.* **2005**, *21*, x15.

(18) Bond lengths of 2.29 and 2.11 Å for $Pd^{II}$−Cl trans to N and $Pd^{II}$−N trans to Cl in *cis*-[$PdCl_2${$Te(CH_2CH_2NMe_2)_2$}]: Dey, S.; Jain, V. K.; Knoedler, A. *Anal. Sci.* **2004**, *20*, x127.

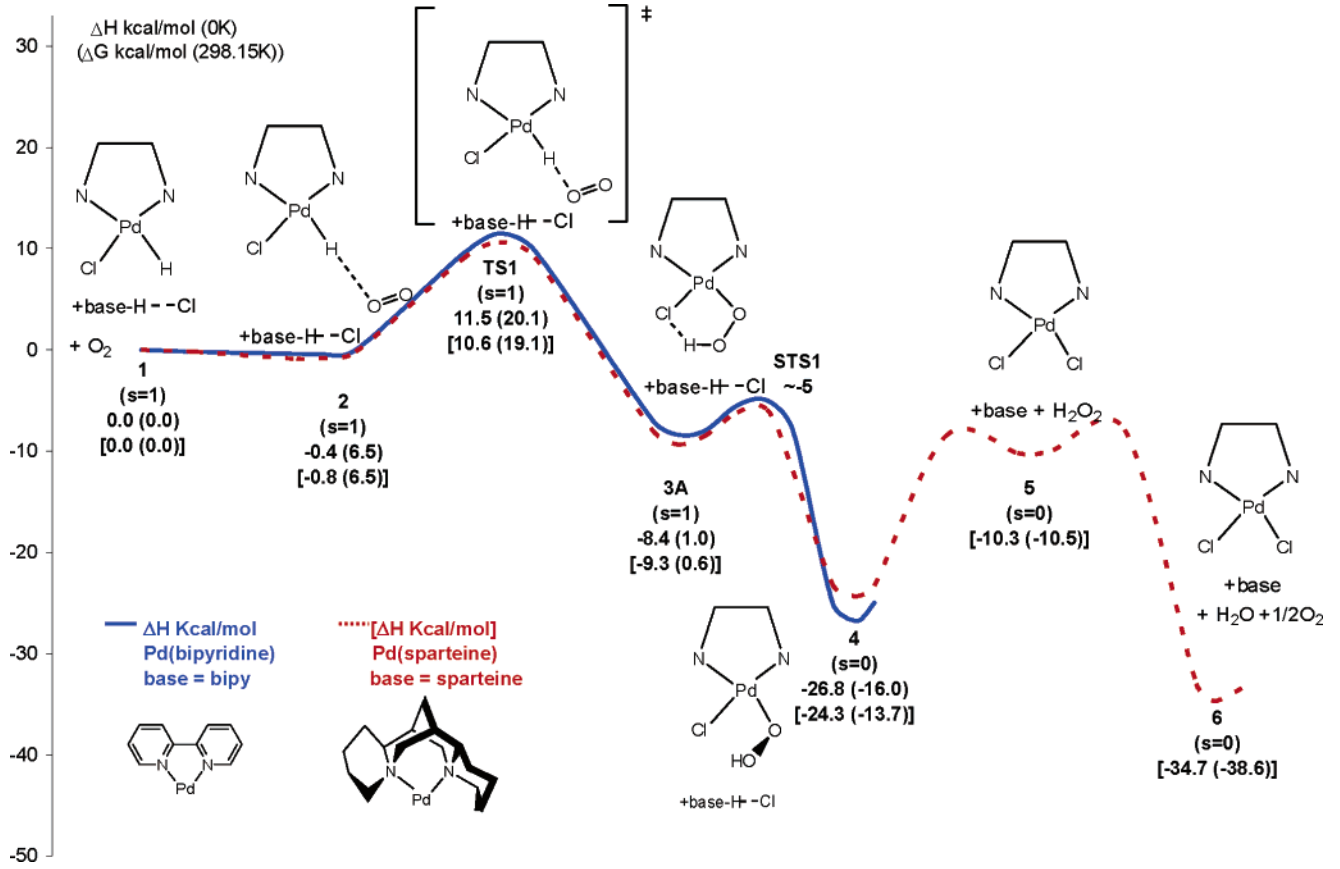


***Figure 4.*** Calculated mechanism for $O_2$ insertion in Pd(L)(H)(Cl) in toluene (L = bipy, [spar]). The upper numbers refer to the solid (blue) energies using bipy as the base, while the lower numbers in brackets and the dotted (red) line use sparteine as the base. The first numbers are $\Delta H$, while the numbers in parentheses are $\Delta G$.

case protonated sparteine, spar-H), which yields **5**, $PdCl_2$, and $H_2O_2$. This process is energetically uphill by 14.0 kcal/mol. Even though this step is endothermic, the strongly exothermic disproportionation of $H_2O_2$ to water and $O_2$ is believed to be sufficient to drive the reaction forward. The mechanism for the conversion of **4** to **5** is well documented and not presented here.[19]

**3.2. Pd(bipyridine) Mechanism.** Further studies were conducted to confirm our expectation that **3A** can easily undergo a spin transition and to explore the rearrangement that connects **TS1** with **3A**. However, to reduce the costs of such calculations, we replaced the sparteine ligand in Pd(sparteine)$(Cl)_2$ with a significantly smaller analogue, Pd(bipyridine)$(Cl)_2$.[20] Bipyridine (bipy) was chosen as a simple cis-restricted bidentate diamine ligand partly to maintain some of the structural restrictions of (−)sparteine, and partly to provide a more general model applicable to a broad range of systems. While Pd(bipy)$(Cl)_2$ has been shown experimentally to *not* be a competent catalyst for the aerobic oxidation of alcohols,[21] our previous computational results indicate that this is due to difficulties in the deprotonation of the alcohol[22] and does thus not imply an inability for Pd(bipy)(Cl)(H) to react with $O_2$. Furthermore, as illustrated in Figure 4 (solid line), the energetic profiles of the bipy and sparteine systems are very similar. We thus believe bipy to be a good ligand substitute for the larger sparteine.

**3.3. Spin Transition.** As mentioned above, a key concern of the insertion mechanism is whether a spin transition between structures **3A** and **4** is feasible. Such "spin-forbidden" processes are fastest when the minimum of the initial state is crossed nearby by the other spin state, to allow metal-mediated spin−orbit coupling. Crossings of different spin-state surfaces are difficult to predict because of spin dependence of correlation energies and DFT functionals. However, the barrier can be estimated by finding the minimum energy crossing point (MECP) between the surfaces, a methodology which Harvey and co-workers showed to adequately model spin-crossings in organometallic systems.[23,24]

We implemented a methodology similar to that used by Harvey to obtain an approximate crossing point. Singlet calculations established that the singlet surface is not accessible prior to **3A**. However, optimization of the singlet starting from the $\mathbf{3A_{bipy}}$ triplet geometry led to structure $\mathbf{4_{bipy}}$, a significantly more stable structure, with the resulting triplet/singlet gap of −18.4 kcal/mol implying spin crossover between $\mathbf{3A_{bipy}}$ and $\mathbf{4_{bipy}}$. The vertical singlet/triplet gap[25] for $\mathbf{3A_{bipy}}$ was calculated to be 9.5 kcal/mol. While too high for a facile crossover, this

(19) (a) Igersheim, F.; Mimoun, H. *Nouv. J. Chim.* **1980**, *4*, 711. (b) Muto, S.; Kamiya, Y. *Bull. Chem. Soc. Jpn.* **1976**, *49*, 2587.
(20) For a similar simplification on the experimental front, see: ten Brink G.-J.; Arends I. W. C. E.; Hoogenraad, M.; Verspui, G.; Sheldon, R. A. *Adv. Synth. Catal.* **2003**, *345*, 497.
(21) Nishimura, T.; Onoue, T.; Ohe, K.; Uemura, S. *Tetrahedron Lett.* **1998**, *39*, 6011.
(22) Keith, J. M.; Nielsen, R. J.; Oxgaard, J.; Goddard, W. A., III. Manuscript in preparation.
(23) Harvey, J. N.; Aschi, M.; Schwarz, H.; Koch, W. *Theor. Chem. Acc.* **1998**, *99*, 95.
(24) Carreón-Macedo, J.-L.; Harvey, J. N. *J. Am. Chem. Soc.* **2004**, *126*, 5789.
(25) Vertical singlet−triplet gap: the difference in energy between the singlet and triplet wave functions with the same geometry.

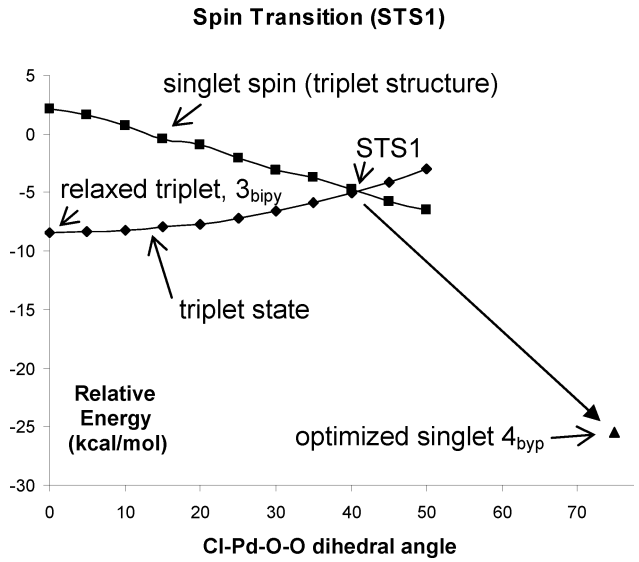


***Figure 5.*** Triplet−singlet spin transition, approximated by varying the Cl−Pd−O−O torsion angle, $\theta$, starting with the stable triplet species **3**, $\theta$ = 0°, until a structure was found in which the singlet and triplet spins had the same gas-phase energy, **STS1**, $\theta$ = ∼41°. Singlet **STS1** was then allowed to relax to product and proceeded directly to species **4**, $\theta$ = 74.9°.

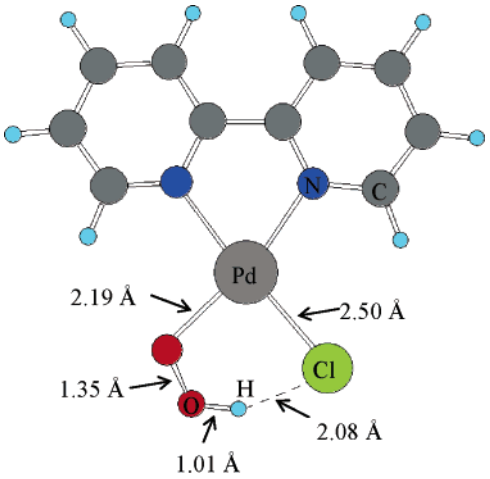


***Figure 6.*** Spin transition-state structure (**STS1**) for spin conversion from triplet to singlet. Here the Cl−Pd−O−O torsion angle is ∼41°.

indicates that $\mathbf{3A_{bipy}}$ and $\mathbf{4_{bipy}}$ must have significantly different geometries since relaxation yields 27.9 kcal/mol. Inspection of the triplet $\mathbf{3A_{bipy}}$ and the singlet $\mathbf{4_{bipy}}$ suggested that the major geometric difference between the two is the torsion angle Cl−Pd−O−O, which goes from 0° in $\mathbf{3A_{bipy}}$ to 74.9° in $\mathbf{4_{bipy}}$.

Consequently, a search for the MECP was undertaken by optimizing triplet structures of $\mathbf{3_{bipy}}$, where the Cl−Pd−O−O torsion angle was constrained at values ranging from the equilibrium position of 0° to larger values within the range of vibrational motion of the molecule (in this case up to 55°), while allowing the rest of the structure to relax. Starting with the $M_S$ = 1 unrestricted triplet-state optimum geometries, we carried out single-point calculations for $M_S$ = 0 by flipping the spin of one orbital and calculating self-consistently. This led to $\mathbf{S}^2$ ranging from 0.000 to 0.020, demonstrating that spin contamination is quite small. We consider these states to accurately describe points on the singlet potential energy surface (Figure 5).

Through this process an intersection was found (Figure 6) with Cl−Pd−O−O torsional angle of ∼41° and an energy 3.6 kcal/mol higher than that of the stable triplet species in the gas phase. In this crossing point the Pd−O bond length of 2.19 Å, the O−O bond distance of 1.35 Å, the H−Cl hydrogen-bonding distance of 2.08 Å, and the O−H bond distance of 1.01 Å are all very similar to those of $\mathbf{3A_{bipy}}$. The only considerable structural differences between this structure and $\mathbf{3A_{bipy}}$ are the Cl−Pd−O−O and Pd−O−O−H torsional angles, and the spin transition point is thus accessible through the vibrational motion of $\mathbf{3A_{bipy}}$.

**3.4. Role of Hydrogen Bonding.** One remaining concern was the possibility that **TS1** did not connect complex **2** with triplet species **3A**. It is not obvious how breaking of the Pd−H bond by $O_2$ results in the formation of the Pd−O−O−H system, and visual inspection of the imaginary frequency showed only a motion of the hydride along the Pd−H−O axis. Intrinsic reaction coordinate calculations from **TS1** were unsuccessful, due to the flatness of the hypersurface. Instead we elected to follow the relaxation of the geometry shortly after the transition state. $\mathbf{TS1_{bipy}}$ was moved slightly along the reaction pathway toward product (the Pd−H bond distance was stretched 0.07 Å from $\mathbf{TS1_{bipy}}$) and then allowed to fully relax. Figure 7 shows the progression of the relaxation from the nudged transition state **A** to product **E**, which corresponds exactly with species $\mathbf{3A_{bipy}}$. Structure **A** is identical to $\mathbf{TS1_{bipy}}$ except for the elongated Pd−H bond; structure **B** exhibits further elongation of the Pd−H distance resulting in the formation of two distinct species, $HO_2^{\bullet}$ and a $Pd^{I}$ T-complex; structure **C** shows the $HO_2^{\bullet}$ moving toward the Cl ligand and forming an H-bond; structure **D** show the $HO_2^{\bullet}$ rotating in order to bring the Pd and O closer together while maintaining the H-bond; finally, structure **E** shows the formation of the Pd−O bond and the formation of the triplet product. This progression demonstrates that the hydrogen bonding which is important for stabilization of **3A** is also important for the formation of **3A** from **TS1**.

Since relaxation from the transition state is not conclusive proof of an uninterrupted pathway, we also elected to investigate the mechanism of a non-hydrogen-bonding analogue, Pd(bipy)-($CH_3$)(H) (see Figure 8). When the transition state in this case is nudged toward products and relaxed, as discussed above, the $-CH_3$ species does not proceed to the expected product $\mathbf{3A_{bipy}}$-$\mathbf{CH_3}$, but instead forms complex $\mathbf{3B_{bipy}}$-$\mathbf{CH_3}$, at 12.8 kcal/mol. $\mathbf{3B_{bipy}}$-$\mathbf{CH_3}$ can be described as a $Pd^{I}$ T-complex with unpaired spin in the orbital formerly covalently bonded to the hydride, while the hydrogen in the $^{\bullet}$OOH radical is coordinating to the same orbital in an agostic fashion. Control calculations of a Pd(bipy)(Cl)(OOH) triplet complex with the starting coordinates of the $Pd^{I}$−HOO$^{\bullet}$ moiety taken from $\mathbf{3B_{bipy}}$-$\mathbf{CH_3}$ again optimized to $\mathbf{3A_{bipy}}$-**Cl**, reinforcing our belief that an intermediate $\mathbf{3B_{bipy}}$-**Cl** is not part of the mechanistic pathway.

Having concluded that eliminating the possibility of internal hydrogen bonding changes the mechanism for hydrogen abstraction, we also elected to determine what effect this has for the overall mechanism. A transition state for the conversion of $\mathbf{3B_{bipy}}$-$\mathbf{CH_3}$ to $\mathbf{3A_{bipy}}$-$\mathbf{CH_3}$ could not be located, but an upper bound for this process is the infinite dissociation of the $Pd^{I}$ and $^{\bullet}$OOH radicals, calculated to be 19.0 kcal/mol from $\mathbf{1_{CH_3}}$. However, whether $\mathbf{3B_{bipy}}$-$\mathbf{CH_3}$ can convert to $\mathbf{3A_{bipy}}$-$\mathbf{CH_3}$ appears to be a moot point. $\mathbf{3A_{bipy}}$-$\mathbf{CH_3}$ is surprisingly high in energy, 12.0 kcal/mol higher than $\mathbf{1_{CH_3}}$. This is in contrast to $\mathbf{3A_{bipy}}$-**Cl**, which is 8.4 kcal/mol *lower* in energy than $\mathbf{1_{Cl}}$. The

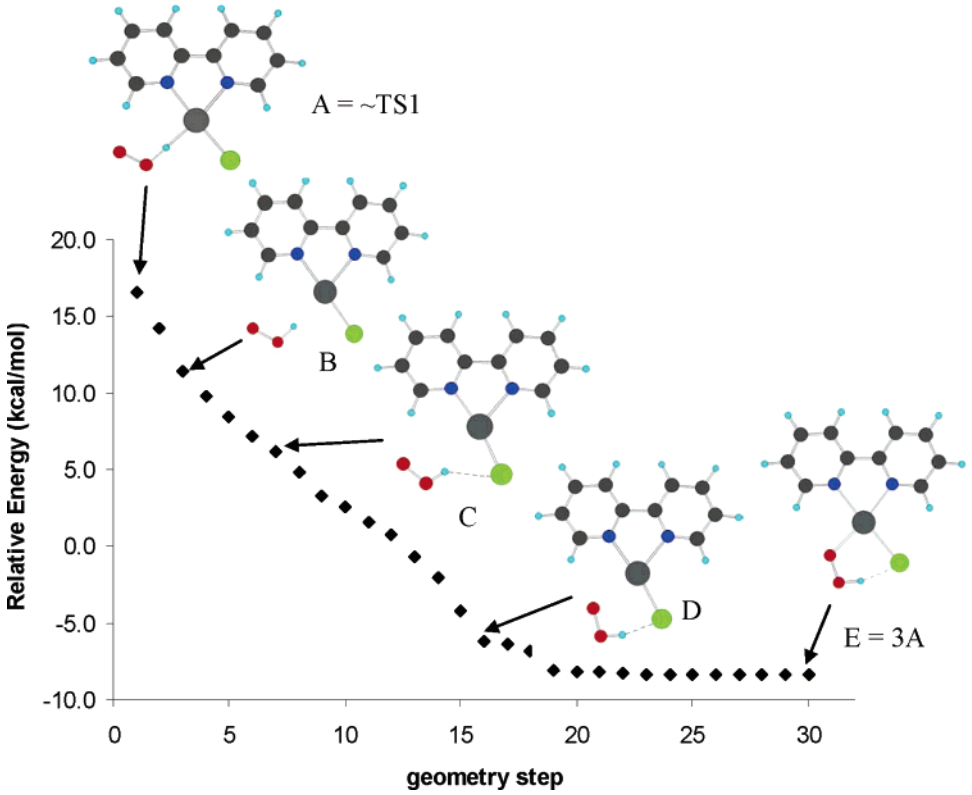


***Figure 7.*** Energetics of the transition-state relaxation reaction pathway from the transition state $\mathbf{TS1_{bipy}}$ (~A) to the stable triplet $\mathbf{3A_{bipy}}$ (E).

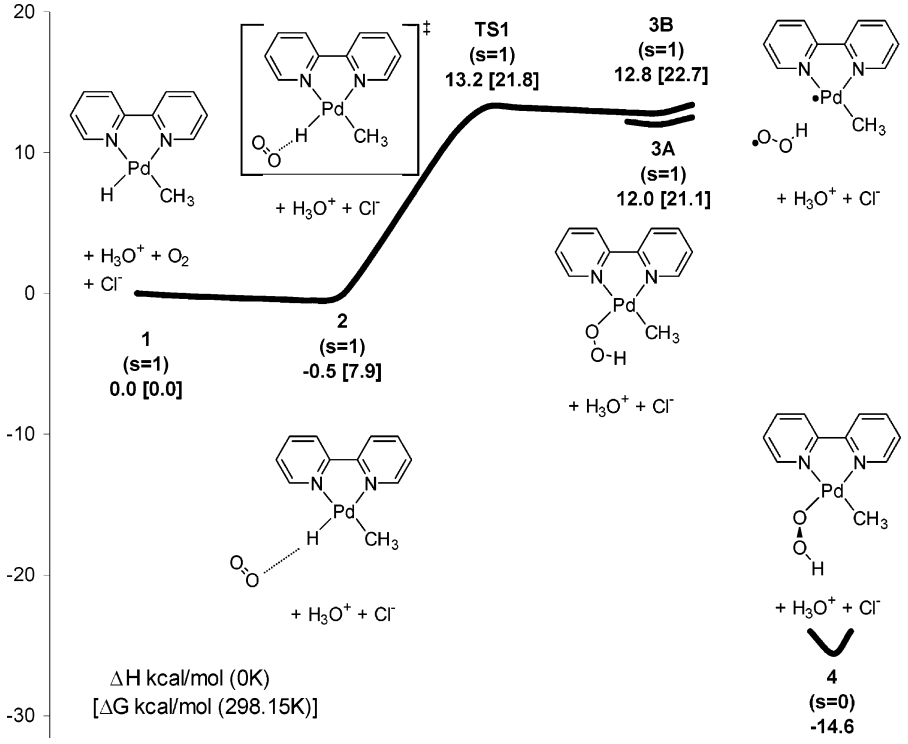


***Figure 8.*** Calculated mechanism for $O_2$ insertion in Pd(bipy)(H)($CH_3$) in $H_2O$.

difference of ~20 kcal/mol is too large to be solely attributed to the lack of hydrogen bonding, estimated at 8−10 kcal/mol. The remaining energy change is most likely caused by the increased $\sigma$-donor ability of the $-CH_3$ substituent, which destabilizes the relatively electron-rich $Pd^I$ complex. Moreover, the increased energy of the $\mathbf{3A_{bipy}\text{-}CH_3}$ triplet pushes it above the $\mathbf{3A_{bipy}\text{-}CH_3}$ singlet, thus causing the spin transition to be inaccessible at this point. Furthermore, since the singlet becomes significantly more stable than the triplet as the mechanism progresses, it is our belief that for this case to proceed through an $O_2$ insertion, the spin transition must occur earlier in the mechanism.

Indeed, calculations show that the relative energy of the $\mathbf{3B_{bipy}\text{-}CH_3}$ *singlet* is 13.2 kcal/mol, i.e., within the margin of

***Table 1.*** $\Delta H$ [$\Delta G$] (kcal/mol) Values for Intermediates and Transition States of the Various Systems Studied

| ligand | X-group | 1 | 2 | TS1 | 3A | 3B | 4 |
|---|---|---|---|---|---|---|---|
| spar | Cl | 0.0 [0.0] | −0.8 [6.5] | 10.6 [19.1] | −9.3 [0.6] | N/A[a] | −24.3 [−13.7] |
| bipy | OAc | 0.0 [0.0] | −0.6 [6.1] | 10.4 [19.0] | −14 [5.3] | N/A[a] | −30.0 [−18.7] |
| bipy | Cl | 0.0 [0.0] | −0.4 [6.5] | 11.5 [20.1] | −8.4 [1.0] | N/A[a] | −26.8 [−22.7] |
| bipy | I | 0.0 [0.0] | −0.7 [6.5] | 12.3 [20.5] | −4.6 [4.9] | N/A[a] | −24.6 [−13.7] |
| bipy | CN | 0.0 [0.0] | −0.6 [6.5] | 13.5 [22.3] | 3.0 [12.1] | N/A[a] | −23.4 [−12.8] |
| bipy | $CF_3$ | 0.0 [0.0] | −0.5 [5.5] | 13.5 [21.0] | 7.0 [14.5] | N/A[a] | −26.0 [−14.7] |
| bipy | $CH_3$ | 0.0 [0.0] | −0.5 [7.9] | 13.2 [21.8] | 12.0 [21.1] | 12.8 [22.7] | −25.6 [−14.6] |

[a] Unstable with respect to **3A**.

***Table 2.*** Optimized $\Delta H$ [$\Delta G$] (kcal/mol) Values for Intermediates and Transition States of the Various Systems Studied

| functional | basis set | 1 | 2 | TS1 | 3A | 4 |
|---|---|---|---|---|---|---|
| B3LYP | LACVP**[a] | 0.0 [0.0] | −0.4 [6.5] | 11.5 [20.1] | −8.4 [1.0] | −26.8 [−16.0] |
| B3LYP | LACV3P**++ | 0.0 [0.0] | −0.1 [4.5] | 11.9 [20.5] | −7.3 [0.4] | −24.5 [−14.1] |
| BLYP | LACVP**[a] | 0.0 [0.0] | −1.9 [5.9] | 5.7 [13.8] | −9.3 [1.4] | −27.6 [−17.1] |
| BP86 | LACVP**[a] | 0.0 [0.0] | −0.4 [7.1] | 4.6 [14.4] | −9.5 [0.6] | −28.8 [−18.3] |

[a] Diffuse functions added to Cl.

error identical to the $\mathbf{3B_{bipy}\text{-}CH_3}$ triplet. This is not unexpected, since the two unpaired spins in $\mathbf{3B_{bipy}\text{-}CH_3}$ are essentially disconnected. Even so, the strong spin−orbit coupling of the Pd atom should facilitate the spin crossing, and we do not expect the barrier to be prohibitively high. Conversion of the $\mathbf{3B_{bipy}\text{-}CH_3}$ singlet to $\mathbf{4_{bipy}\text{-}CH_3}$ should occur via a mechanism similar to the conversion of triplet **3B** → **3A**, and thus has an upper bound barrier of 19.0 kcal/mol. With a barrier to activation between 13.6 and 19.0 kcal/mol, the reaction is expected to be feasible, but significantly slower than the analogous reaction with the −Cl species.

Further insight into the H-bonding effects is obtained by comparison of structures **1**, **2**, **TS1**, **3**, and **4** with a variety of ligands of varying electronic properties (Table 1). It can easily be seen that as the X-ligand's ability to accept a hydrogen bond is reduced and then completely eliminated through the substitution from ligands such as OAc, Cl, and I to ligands like CN, $CF_3$, and finally $CH_3$, the energy of **3A** is increased with respect to all the other species.

**3.5. Comparison of Computational Methodologies.** To ensure that the results described here are not artifacts caused by the particular methodology employed, we optimized the geometries of **1**, **2**, **TS1**, **3A**, and **4** using B3LYP with a triple-$\zeta$ basis set (LACV3P**++) as well as two other density functionals (BLYP and BP86). The results are summarized in Table 2, where it can be seen that the use of the larger basis set changes the energies very little. The largest change on the $\Delta H$ surface is for **1** → **4**, which is exothermic by −26.8 kcal/mol using LACVP** and −24.5 kcal/mol using LACV3P**++. The changes on the $\Delta G$ surface mimic the changes on the $\Delta H$ surface and do not warrant further comment. The BLYP and BP86 surfaces correspond very closely to the B3LYP surface, with the exception of the transition state **TS1**. The calculated BLYP $\Delta H^{\ddagger}$ is 5.7 kcal/mol with respect to **1** and 7.6 kcal/mol with respect to **2**, while the BP86 $\Delta H^{\ddagger}$ is 4.6 and 5.0 kcal/mol, respectively. This is compared to the B3LYP $\Delta H^{\ddagger}$, which is calculated to be 11.5 and 11.9 kcal/mol, respectively. The B3LYP barrier is roughly twice as high as the BLYP and BP86 barriers. However, it should be noted that BP86 is known to yield lower barriers than B3LYP, and there is some indication that the B3LYP barrier corresponds better to experimental values.[26]

## 4. Conclusions

A direct insertion of triplet $O_2$ into $Pd^{II}$ hydride to form a final singlet state is accessible with certain limitations. The reaction proceeds through abstracting the hydrogen from palladium by $O_2$, which in our case immediately forms a hydrogen bond with the neighboring X-type ligand. The H-bonded complex relaxes to a triplet $Pd^{I}$−OOH species, which subsequently undergoes a spin transition to the corresponding singlet $Pd^{II}$−OOH. This singlet species is then protonated, and hydrogen peroxide is replaced by another X-type ligand to complete the catalytic cycle. The limitations involved in the spin transition, the formation of the triplet $Pd^{I}$−OOH species, and the stability of that triplet species are all dependent on the presence of a H-bond acceptor cis to the hydride and the electronic characteristics of the other ligands which may or may not stabilize the $Pd^{I}$ species. Without this cis H-bond acceptor and/or electron-withdrawing ligands that can stabilize $Pd^{I}$, the reaction will not proceed via the palladium hydride insertion mechanism. We are now building on these results to focus on evaluating the $Pd^{0}$ mechanisms (eqs 1 and 2) using known catalysts in order to compare relative barriers in systems where the direct insertion mechanism is feasible.

**Acknowledgment.** J.M.K. thanks the National Science Foundation for financial support. This research was partly funded by the NSF (CTS-01322002) and ChevronTexaco, and the facilities used were funded by grants from ARO-DURIP, ONR-DURIP, IBM-SUR, and the Beckman Institute.

**Supporting Information Available:** Tables of geometries, ZPE corrections, and absolute energies of intermediates, as well as geometries, ZPE corrections, absolute energies, and imaginary frequencies of transition states. This material is available free of charge via the Internet at http://pubs.acs.org.

JA043094B

(26) Fan, Y.; Hall, M. B. *Chem. Eur. J.* **2004**, *10*, 1805.